ISSN: 2414-1895 DOI: 10.6919/ICJE.202506_11(6).0026

Characteristic Analysis and Optimization Design of Permanent Magnet Synchronous Motor with New Rotor Structure

Xuanfeng Shangguan, Yu Xie, Xin Wang, and Qi Wang

Henan Polytechnic University, Jiaozuo 454003, China

Abstract

In order to solve the problem that the traditional surface-mount permanent magnet synchronous motor (SPMSM) is difficult to effectively utilize the reluctance torque, a new rotor structure based on bonded magnets is studied. By optimizing the shape design of the bonded magnet and using a non-circular cross-section shaft, the SPMSM generates convex polarity, and realizes the synergistic utilization of electromagnetic torque and reluctance torque. Theoretical analysis shows that the structure can obtain the maximum electromagnetic torque and reluctance torque at the same time under the same current phase. The simulation results based on the finite element method show that the output torque of the new rotor structure motor is increased by about 14% compared with the traditional structure under the condition of keeping the volume of the permanent magnet and the driving current unchanged. This study provides a new idea for improving the torque output performance of SPMSM, and has important reference value for the development of next-generation high-performance SPMSM.

Keywords

Bonded Magnets; Convex Polarity; Reluctance Torque; Surface-Mount Permanent Magnet Synchronous Motor.

1. Introduction

Due to its high power density, high efficiency and high reliability, permanent magnet synchronous motors have been widely used in industrial drives, new energy vehicles and wind power generation. Among them, SPMSM has become one of the hotspots in research and application due to its simple structure, low manufacturing cost, and convenient control[1]. However, with the continuous improvement of motor performance requirements in application scenarios, traditional SPMSM faces many challenges in terms of torque density, torque ripple, and operating efficiency [2].

In terms of torque performance, the torque density of traditional SPMSM is limited by the rotor structure and permanent magnet material, which is difficult to meet the needs of high-performance drive systems[3]. In addition, due to the non-uniformity of the magnetic field distribution of permanent magnets, SPMSM is prone to large torque ripples during operation, resulting in vibration and noise problems, affecting the stability and reliability of the system[4]. In order to solve these problems, scholars at home and abroad have proposed a variety of new rotor structures and optimization design methods in recent years. For example, by changing the shape and arrangement of permanent magnets, or by introducing an auxiliary slot structure, the torque density can be effectively increased and torque ripple can be reduced[5-6]. In Ref. [7], a magnetic pole shape optimization method based on analytical calculation was proposed, which effectively reduced the waveform distortion rate of air gap magnetic flux density. In Ref. [8], a new magnetic pole structure with convex pole shoes on surface-mount rectangular permanent magnet steel was proposed to improve the output performance of the motor. A torque enhancement scheme using an axial-assisted magnet was proposed in Ref. [9]. In Ref. [10],

ISSN: 2414-1895 DOI: 10.6919/ICJE.202506_11(6).0026

a quasi-ironless SPMSM using carbon fiber reinforced plastic (CFRP) and a small amount of soft magnetic composite (SMC) cores was studied to reduce the weight of electric motors.

Based on the new rotor structure proposed in Ref. [11], a new rotor structure SPMSM is designed, which uses the shape plasticity of the bonded magnet and adopts a non-circular cross-section shaft to generate convex polarity of the motor, and the output torque of the SPMSM is increased by using reluctance torque. On the premise of ensuring the manufacturing cost and process feasibility, the output torque of the motor is significantly improved. Based on finite element simulation, the torque characteristics of the new rotor structure motor are verified, and the effectiveness and practicability of the new structure are verified by comparing and analyzing with the traditional SPMSM.

2. SPMSM Principle and Torque Characteristics of New Rotor Structure

2.1 SPMSM Topology and Principle of New Rotor Structure

In this paper, a novel rotor structure high-speed permanent magnet synchronous motor is studied, which utilizes the reluctance torque by using the shape freedom of the bound magnet to provide the maximum output torque in the same phase. The radial profile of the new rotor structure permanent magnet synchronous motor is shown in Figure 1, the rotor sheath is made of carbon fiber material to reduce eddy current loss, the bonded magnet is filled between the shaft and the sheath, the rotor core is not used, and the shaft is processed into an oval or other irregular shape by using the shape plasticity of the bonded magnet.

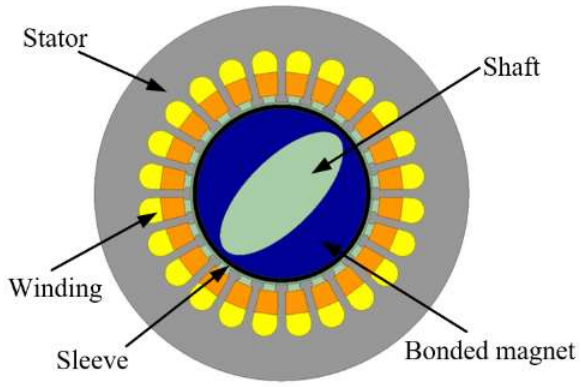

Figure 1. Schematic diagram of the radial profile of a new rotor structure permanent magnet synchronous motor

Using the high degree of freedom of the shape of the bonded magnet, it is possible to assemble a magnet with relatively complex shapes in space, and Figure 2 is a schematic diagram of the new rotor structure studied in this paper. The new rotor structure is characterized by the use of axes with an elliptical cross-section, with long and short directions, rather than circular cross-sections.

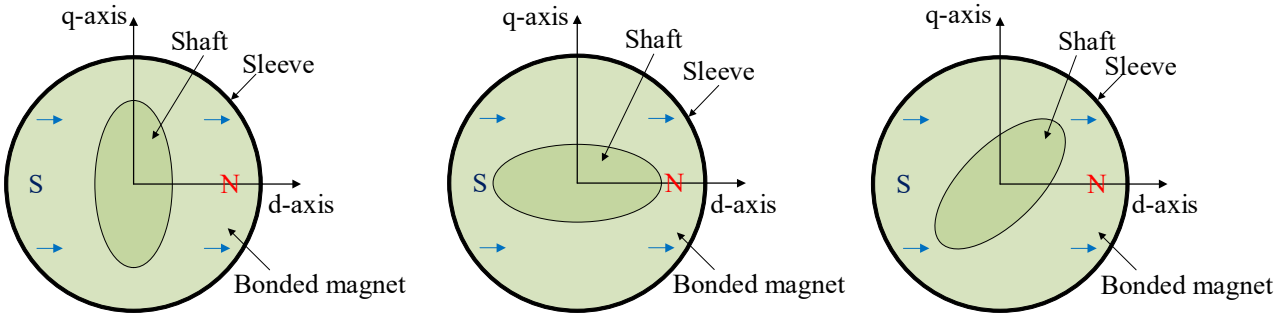

Figure 2. Schematic diagram of the new rotor structure

ISSN: 2414-1895 DOI: 10.6919/ICJE.202506_11(6).0026

In built-in permanent magnet synchronous motors, the rotor structure naturally has salient pole characteristics, so that the reluctance torque can be fully utilized. However, in conventional surface-mount permanent magnet synchronous motors, the magnetic resistance of the D-axis and the Q-axis is almost the same, making it difficult to generate reluctance torque.

Fig. 2(a) is the rotor structure of a surface-mount permanent magnet synchronous motor with reverse convex polarity, with a truncated length along the q-axis than a truncated long shaft along the d-axis, and the magnetic resistance in the d-axis direction of the rotor is less than that in the q-axis direction (i.e., $L_d<L_q$), which can produce reluctance torque in the current phase of weakening the magnetic field, and the motor needs to weaken the magnetic field during operation, which will cause a certain risk of demagnetization to the magnet, especially for the bonded magnet with low demagnetization resistance; Fig. 2(b) is the rotor structure of a surface-mount permanent magnet synchronous motor with positive convex polarity, the truncated length along the d-axis is longer than the truncated length along the q-axis, and the magnetic resistance in the q-axis direction of the rotor is less than that in the d-axis direction (i.e., $L_d>L_q$), which can produce reluctance torque under the current phase of the enhanced magnetic field, and does not need to weaken the magnetic field. Fig. 2(c) shows the rotor structure of the surface-mount permanent magnet synchronous motor studied in this paper, the salient pole of the shaft is located at a position of 45° away from the d-axis, and the maximum electromagnetic torque and maximum reluctance torque are achieved at the same current phase.

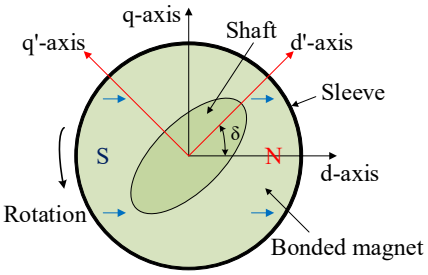

Figure 3. Definition of the salient pole of the motor

As shown in Figure 3, the phase difference between the d' axis and the d-axis is defined as δ. The shape freedom of the bonded magnet realizes the convexity of the asymmetrical cross-section shaft, and the reluctance torque can be used even in surface-mount high-speed permanent magnet synchronous motors. Moreover, the salient axis can be set freely with respect to the d-axis.

2.2 Torque Characteristics of Permanent Magnet Synchronous Motor with New Rotor Structure

The vector diagram of the current phase β defined in this paper is shown in Figure 4, where β is the current phase, ψ_a is the magnetic flux, L_d and i_d are d-axis inductance and current, L_q and i_q are q-axis inductance and current, ω is angular velocity, and i_a is phase current.

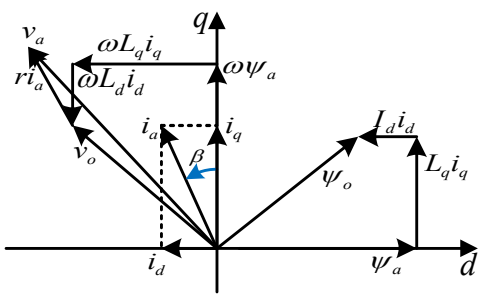

Figure 4. The current phase β defines a vector diagram

ISSN: 2414-1895 DOI: 10.6919/ICJE.202506_11(6).0026

The expected torque characteristics of the new high-speed permanent magnet synchronous motor are shown in Figure 5, where τ_m is the electromagnetic torque, τ_r is the reluctance torque, and τ is the total torque.

Figure 5(a) shows the torque characteristics of the motor at δ=90º, with the maximum electromagnetic torque at β=0º and the maximum reluctance torque at β=45º. Figure 5(b) shows the torque characteristics of δ=0º, again at β=0º the maximum electromagnetic torque and at β=−45º. Figure 5(c) shows the torque characteristics at δ=45º, with the maximum electromagnetic torque and maximum reluctance torque generated along the q-axis at the same current phase β=0º, and the output torque per ampere current is maximum.

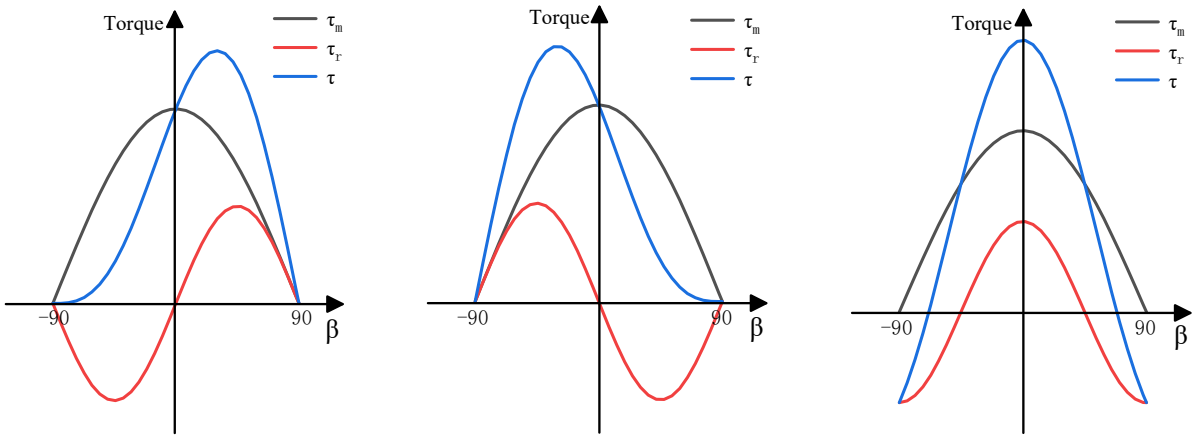

(a) δ=90º (b) δ=0º (c) δ=45º

Figure 5. Diagram of expected torque characteristics of a new high-speed permanent magnet synchronous motor

When the direction of the shaft salient pole coincides with the D axis or the Q axis, i.e., when δ=90º or δ=0º, the total torque of the motor

$$\tau = P_n\left[\Psi_a i_a \cos\beta + \frac{1}{2}\left(L_q - L_d\right) i_a^2 \sin 2\beta\right] \tag{1}$$

where P_n is the number of pole pairs, ψ_a is the magnetic flux, i_a is the phase current, L_q is the q-axis inductance, and L_d is the d-axis inductance.

When the salient pole direction is between the d-axis and the q-axis (90º>δ>0º), the difference between L_d and L_q cannot be used as a source of reluctance torque because the phase of the inductance peak is inconsistent with the d-axis and the q-axis, and Eq. (1) does not apply to the salient pole direction between the d-axis and the q-axis (90º>δ>0º) of the motor's torque characteristics. The reluctance torque is proportional to the difference between $L_{d'}$ and $L_{q'}$, and its phase is affected by the δ, where $L_{d'}$ is the d′ axis inductance and $L_{q'}$ is the q′ axis inductance, as shown in Eq. (2). Let δ=45º, Eq. (2) equals Eq. (3). In this case, both the magnet torque and the reluctance torque reach their maximum at β=0º, as shown in Eq. (3).

$$\tau = P_n\left[\Psi_a i_a \cos\beta + \frac{1}{2}\left(L_{q'} - L_{d'}\right) i_a^2 \sin 2(\beta - \delta)\right] \tag{2}$$

ISSN: 2414-1895 DOI: 10.6919/ICJE.202506_11(6).0026

$$\tau = P_n\left[\Psi_a i_a \cos\beta + \frac{1}{2}\left(L_{q'} - L_{d'}\right) i_a^2 \sin 2\left(\beta - \frac{\pi}{4}\right)\right] \tag{3}$$

3. Finite Element Simulation Verification

3.1 Motor Design Indicators

Since this paper needs to verify the torque characteristics of three salient shaft motors with different angles, and also needs to compare the performance with the basic structure motors, four motors are designed in this paper, with a rated power of 10kW and a rated speed of 30,000rpm. In order to weaken the harmonic electromotive force and harmonic magnetokinetic potential, the motor adopts double-layer short-distance distributed winding, combined with the working condition of the motor in this paper and the consideration of material cost, the permanent magnet is made of bonded ferrite material, and the traditional circular cross-section shaft motor is the basic motor, and the new type of salient shaft with δ=90º, δ=0º, and δ=45º are motor A, motor B, and motor C, so as to ensure that the amount of permanent magnets and other parameters of the four motors remain unchanged, and only the shape of the rotating shaft is changed. Through the calculation and analysis in Chapter 2, the specific structural parameters of the four motors are shown in Table1.

Table 1. Three Scheme comparing

Parameter	Unit	Basic motor	Motor A	Motor B	Motor C
Number of pole pairs		2			
Number of slots		24			
Salient pole direction	Deg	/	90	0	45
Stator outer diameter	mm	80			
Joko inner diameter	mm	40			
Bond magnet thickness	mm	7	/		
Circular shaft outer diameter	mm	14	/		
Elliptical pivot major axis	mm	/	16.5		
Elliptical pivot minor axis	mm	/	8		
The length of the air gap	mm	0.5			
Sheath thickness	mm	1			

3.2 Simulation of Basic Motor Performance

The electromagnetic finite element simulation software ANSYS Electronics Desktop was used to generate a two-dimensional simulation model according to the structural parameters of the electromagnetic design of the motor, and the appropriate finite element mesh, magnetic field simulation constraints and excitation source conditions were set to complete the electromagnetic field finite element simulation. This section mainly compares and analyzes the basic motor and motor C to study the difference in performance.

ISSN: 2414-1895 DOI: 10.6919/ICJE.202506_11(6).0026

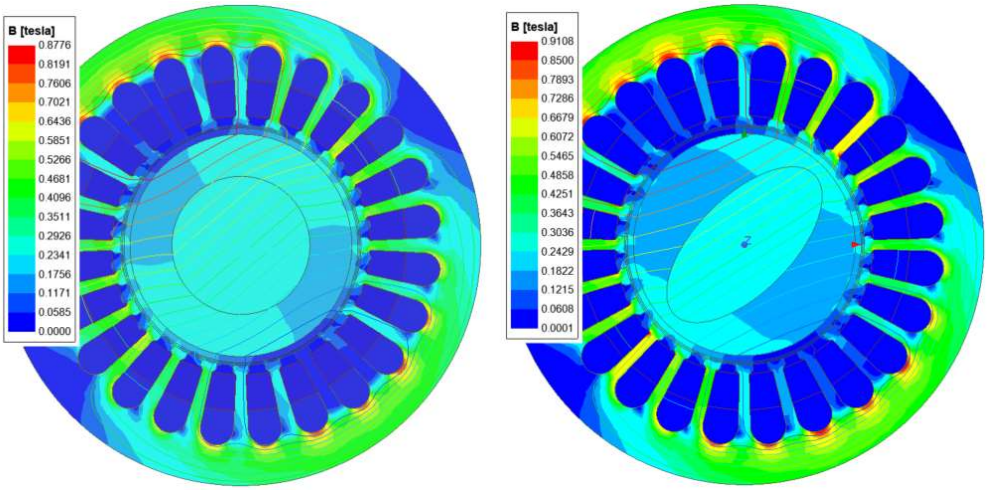

(a) Infrastructure (b) Motor A

Figure 6. Motor magnetic dense cloud diagram

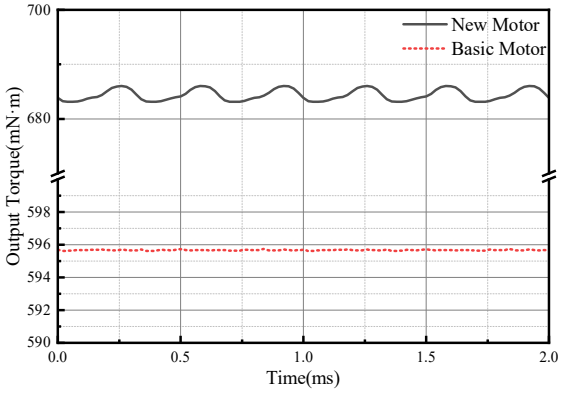

Figure 7. Output torque

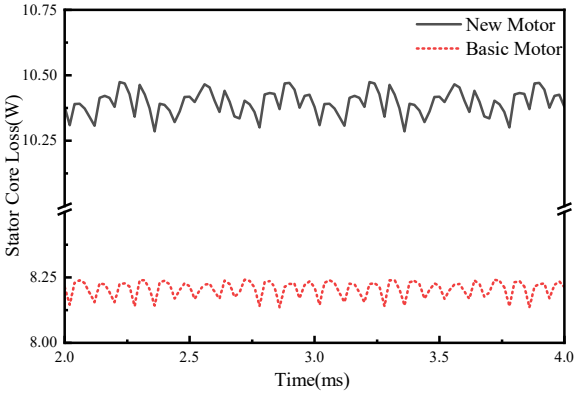

Figure 8. Stator iron consumption

Using the constructed two-dimensional model, the magnetic flux density contour of the basic structure motor and the new structure permanent magnet synchronous motor obtained by simulation is shown in Figure 6. The magnetic density of the stator yoke of the motor is only about 0.9T, which is lower than the saturation point of 1.40T of silicon steel sheet material, which is caused by the weak magnetic magnetism of bonded ferrite.

The comparison of the torque waveforms of the two motors calculated by simulation is shown in Figure 7, the average output torque of the new motor is 683.33mN·m, the average output torque of the basic motor is 595.67 mN·m, the average output torque of the new motor is increased by 14.71% compared with the basic motor, and the peak torque ripple of the new motor is 2.95mN·m, which is about 4‰ of the average output torque. The output torque stability is stronger than that of the new motor; Figure 8 shows the comparison of stator iron consumption of the two motors during stable operation, and it can be seen from the figure that the stator iron consumption of the basic motor is significantly lower than that of the new motor. Specifically, the iron consumption value of the new motor fluctuates between 10.25W and 10.5W, while the iron consumption value of the basic motor fluctuates between 8.1W and 8.25W, which indicates that the core material utilization rate of the basic motor is higher and the magnetic field distribution is more uniform.

3.3 Finite Element Simulation Verification of Torque Characteristics

The four rotor structure permanent magnet synchronous motors shown in Figure 1 and Figure 2 are modeled and simulated respectively, all using the same electrical load and permanent magnet consumption, and the torque characteristics of the three new rotor structures are compared with the

ISSN: 2414-1895 DOI: 10.6919/ICJE.202506_11(6).0026

traditional basic structure, and the output torque characteristics and reluctance torque characteristics of the four motors are shown in Figure 9 and Figure 10 respectively.

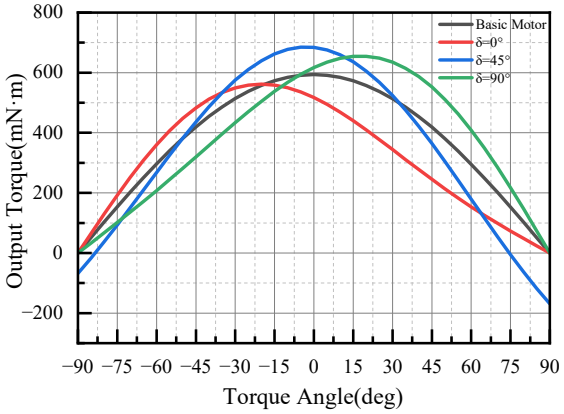

Figure 9. Output torque characteristics

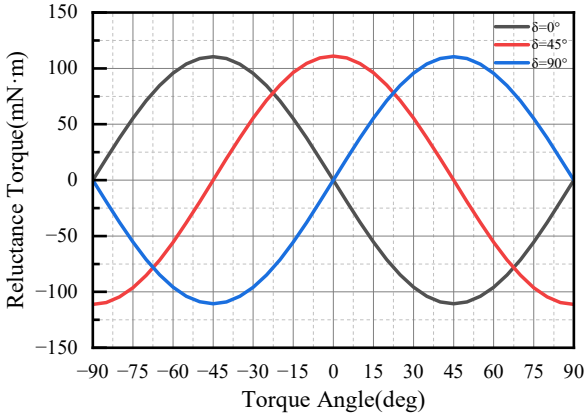

Figure 10. Reluctance torque characteristics

It can be seen from the analysis of Fig. 9 and Fig. 10 that when the salient pole direction of the motor coincides with the q-axis (i.e., δ=90º), the electromagnetic torque is higher due to the large volume of the magnet in the d-axis direction, and the maximum reluctance torque is generated at β=45º due to the reverse salient pole structure of the motor, and the peak torque angle of the output torque is shifted to the right, which is improved compared with the traditional basic structure motor; When the salient pole direction of the motor coincides with the d-axis (i.e., δ=0º), the peak output torque shifts to the left and decreases slightly, although the motor is a positive salient pole structure, and the maximum reluctance torque is generated at β=−45º, due to the small volume of the magnet in the D-axis direction, the electromagnetic torque decreases, resulting in the phenomenon that the output torque is slightly lower than that of the traditional traditional basic structure motor. When the salient pole direction of the motor is 45° between the d-axis and the q-axis (i.e., δ=45º), the peak electromagnetic torque and the peak reluctance torque of the motor occur at the same time at β=0º, and the output torque is significantly improved compared with the traditional basic structure motor.

Through finite element analysis, it is verified that the new rotor structure motor can effectively use the reluctance torque, so as to significantly improve the output torque of the motor, especially when the salient pole direction of the motor is 45° between the d-axis and the q-axis, the maximum magnetic torque and the maximum reluctance torque can be generated at the same time in the same current

ISSN: 2414-1895 DOI: 10.6919/ICJE.202506_11(6).0026

phase, which makes the output torque increase by 14.21% compared with the traditional basic structure motor, which provides an important theoretical basis and technical support for the development of high-performance permanent magnet synchronous motor.

4. Optimized Design of the Motor

Because the torque fluctuation of the motor studied in this paper is small and is in a reasonable range, the output torque and stator iron consumption are selected as the optimization objectives to optimize the structural parameters of the motor. Under the condition of keeping the current load unchanged, the notch width b_{s0}, the elliptical rotating shaft long axis length a, the bottom width of the groove b_{s2}, the stator outer diameter D_o and the groove depth h_s were selected as the optimization variables. Before the motor optimization, the parameters of a single optimization variable are changed to understand the specific influence of different parameters on the motor, so as to lay a good foundation for the optimization work.

4.1 The Influence of Different Parameters on the Motor

Under the condition of keeping the other parameters of the motor unchanged, only one optimization variable is changed at a time, and the relationship curve between each optimization variable and the optimization target is shown in Figure 11.

As can be seen from Figure 11(a), with the increase of the notch width b_{s0}, the output torque of the motor and the iron consumption of the stator are reduced. Because the increase in the width of the notch leads to an increase in the magnetic resistance of the air gap, which in turn weakens the strength of the air gap magnetic field, it will directly affect the output torque of the motor and reduce it. Secondly, the stator iron loss is mainly composed of hysteresis loss and eddy current loss, when the width of the notch is too large, the strength of the air gap magnetic field is weakened, the magnetic flux density is reduced, and the iron loss will be reduced.

As can be seen from Figure 11(b), the output torque of the motor and the iron loss of the stator both increase significantly with the increase of the length a of the long axis of the elliptical rotating shaft. Under the condition of not changing the amount of permanent magnets, the cross-sectional area of the elliptical rotating shaft should be the same, and the increase of the long axis length is accompanied by the decrease of the short axis length, which makes the convexity of the motor more prominent, and increases the output torque of the motor by increasing the reluctance torque, but at the same time increases the inhomogeneity of the magnetic flux density distribution and the harmonic magnetic field, resulting in an increase in iron consumption.

Figure 11(c) shows that the output torque and stator iron loss of the motor increase with the width of the bottom of the groove b_{s2} are opposite, but the output torque decreases very small and is negligible, while the stator iron loss increases significantly, which is due to the small change of the air gap magnetic field and magnetic flux leakage, but the non-uniformity of the magnetic flux density distribution in the stator core will increase the local hysteresis loss and eddy current loss.

It can be seen from Figure 11(d) that the output torque of the motor is relatively stable before the stator outer diameter D_o reaches 82mm, and the continuous increase of the outer diameter of the stator will lead to the decrease of torque, while the iron loss of the stator decreases monotonically with the increase of the outer diameter of the stator. When the outer diameter of the stator is small (≤82mm), the change of the air gap magnetic field and the saturation effect of the magnetic circuit is small, but when the outer diameter of the stator continues to increase, the weakening of the air gap magnetic field, the increase of flux leakage and the unsaturation effect of the magnetic circuit lead to the decrease of the output torque. At the same time, the increase of the outer diameter of the stator leads to the decrease of magnetic flux density, the optimization of the volume distribution of the iron core, and the weakening of the harmonic magnetic field, so that the iron loss is monotonically reduced.

As can be seen from Figure 11(e), the output torque of the motor decreases slightly with the increase of the groove depth h_s. The iron consumption of the stator increases sharply with the increase of the

ISSN: 2414-1895 DOI: 10.6919/ICJE.202506_11(6).0026

groove depth h_s. This trend shows that the increase in groove depth has a relatively small impact on the output torque, but there are still some negative effects. This is due to the fact that the increase in the depth of the groove affects the efficiency of the magnetic circuit or the distribution of the magnetic field, which slightly reduces the output of torque. The sharp increase in stator iron loss is due to the increase in the volume of the core due to the increase in the depth of the trough, which significantly increases the hysteresis and eddy current losses in the core, indicating that a larger trough depth leads to higher energy loss. A combination of these factors needs to be taken into account for optimal performance when optimizing at a later stage, and while a larger groove depth may provide better mechanical strength and heat dissipation, it can also result in higher energy losses.

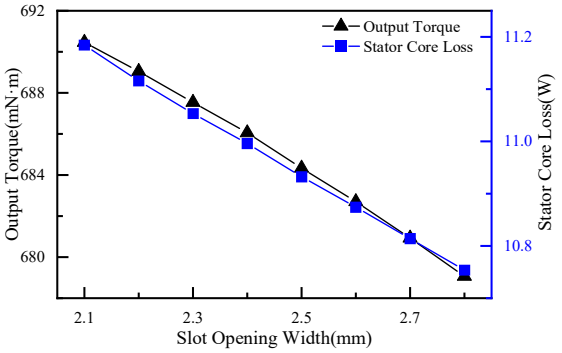

(a) Slot width

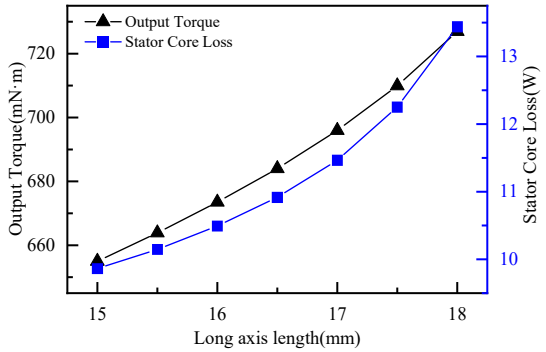

(b) Long axis length

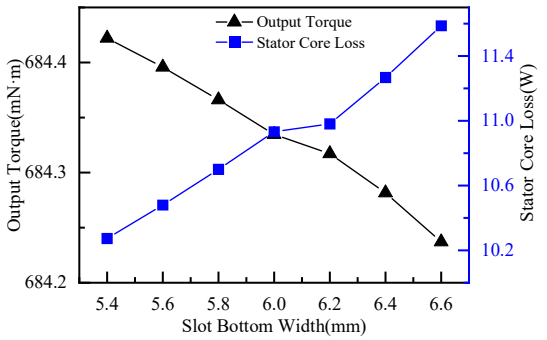

(c) Slot bottom size

ISSN: 2414-1895 DOI: 10.6919/ICJE.202506_11(6).0026

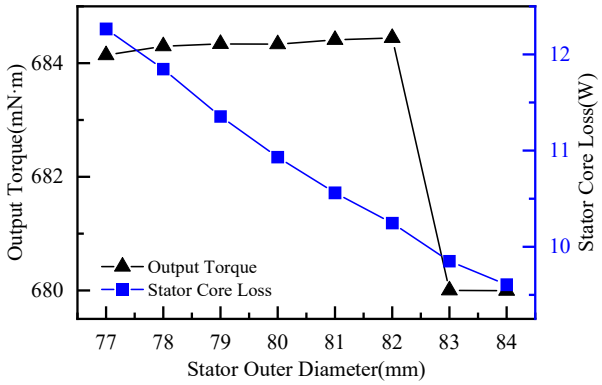

(d) Stator outer diameter

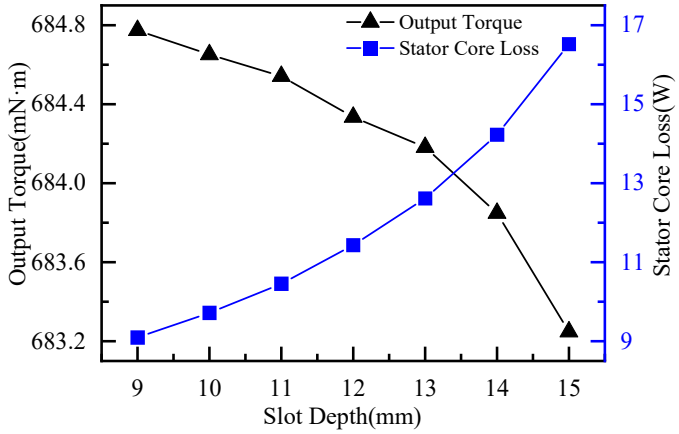

(e) Slot depth

Figure 11. The impact of different variables on the optimization goal

4.2 Multi-objective Optimization based on Taguchi Method

In the optimization process, the amount of permanent magnets is always kept unchanged, the initial parameter values of the given motor are shown in Table 2, the control variable method is selected, 5 horizontal values are selected for each variable as shown in Table 3, and different horizontal values are substituted into the finite element simulation in turn without changing other parameters.

Table 2. Initial parameters of the motor

Optimize variables	Size
b_{s0}/mm	2.5
a/mm	16.5
b_{s2}/mm	6
D_0/mm	80
h_s/mm	12

ISSN: 2414-1895 DOI: 10.6919/ICJE.202506_11(6).0026

Table 3. Horizontal values for different parameters

Optimize variables	b_{s0}/mm	a/mm	b_{s2}/mm	D_0/mm	h_s/mm
Standard 1	2.3	15.5	5.6	78	10
Standard 2	2.4	16	5.8	79	11
Standard 3	2.5	16.5	6	80	12
Standard 4	2.6	17	6.2	81	13
Standard 5	2.7	17.5	6.4	82	14

Table 4. Experimental matrices and finite element calculation results

Test serial number	Trial matrix					F_{ave}	P_{fe}
	b_{s0}/mm	a/mm	b_{s2}/mm	D_o/mm	h_s/mm	/mN·m	/W
1	2.3	15.5	5.6	78	10	666.90	8.85
2	2.3	16	5.8	79	11	676.53	9.84
3	2.3	16.5	6	80	12	687.54	11.05
4	2.3	17	6.2	81	13	699.23	12.51
5	2.3	17.5	6.4	82	14	713.33	14.24
6	2.4	15.5	5.8	80	13	665.15	11.24
7	2.4	16	6	81	14	674.64	12.56
8	2.4	16.5	6.2	82	10	686.31	9.04
9	2.4	17	6.4	78	11	697.81	11.45
10	2.4	17.5	5.6	79	12	711.87	12.48
11	2.5	15.5	6	82	11	664.08	8.75
12	2.5	16	6.2	78	12	673.39	11.33
13	2.5	16.5	6.4	79	13	684.06	12.90
14	2.5	17	5.6	80	14	695.41	14.11
15	2.5	17.5	5.8	81	10	710.28	9.93
16	2.6	15.5	6.2	79	14	661.82	13.52
17	2.6	16	6.4	80	10	672.14	9.04
18	2.6	16.5	5.6	81	11	682.88	9.40
19	2.6	17	5.8	82	12	694.24	10.55
20	2.6	17.5	6	78	13	707.41	14.79
21	2.7	15.5	6.4	81	12	660.91	9.82
22	2.7	16	5.6	82	13	670.22	10.44
23	2.7	16.5	5.8	78	14	679.97	15.33
24	2.7	17	6	79	10	692.49	9.79
25	2.7	17.5	6.2	80	11	705.93	11.13

ISSN: 2414-1895 DOI: 10.6919/ICJE.202506_11(6).0026

In the preliminary optimization of the high-speed permanent magnet synchronous motor with a new rotor structure using the Taguchi method, the orthogonal test involves five optimization variables, each of which has five different horizontal values. The test results obtained by combining the finite element method are shown in Table 4.

In order to analyze the influence of each optimization variable on the output torque and stator iron consumption, the average value of the finite element test results is analyzed, and the average value of the optimization target of each optimization variable at different levels is shown in Figure 12.

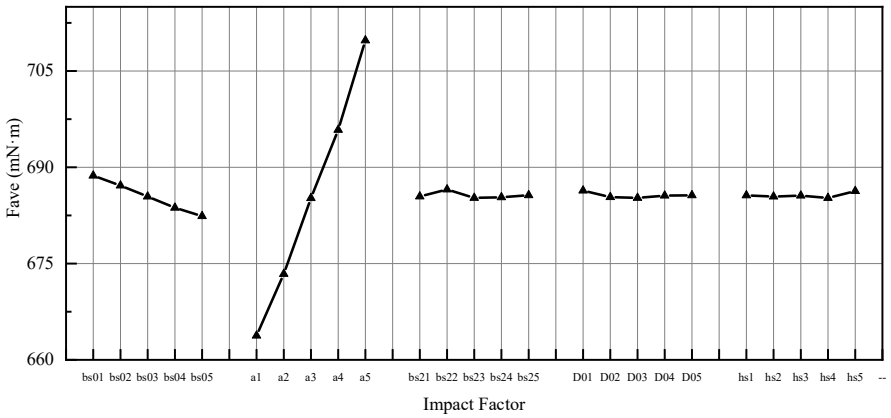

(a) Output torque

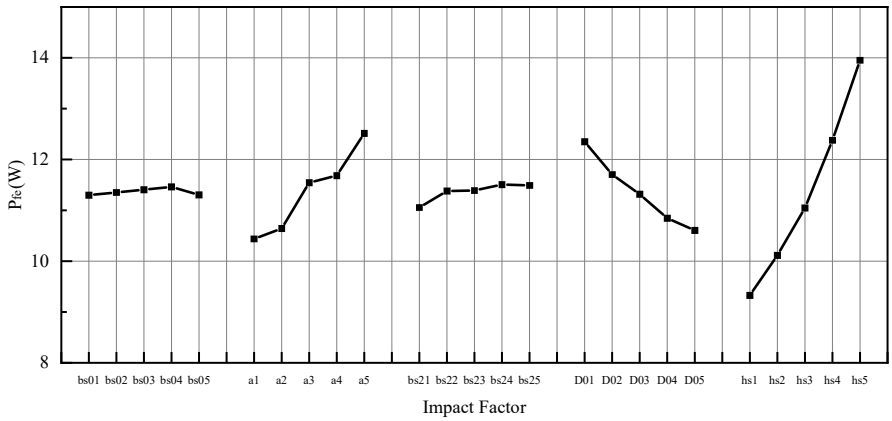

(a) Stator core loss

Figure 12. The average value of the optimization objectives at each factor level for different optimization variables

It can be seen from Fig. 12 that the slot width b_{s0} and the long axis length a of the rotating shaft have a great influence on the output torque of the motor, but the influence of the notch width is relatively small, while the long axis length a of the rotating shaft, the outer diameter of the stator and the depth of the groove hs have a significant impact on the iron consumption of the stator. Considering the main optimization variables, the length of the long axis of the rotating shaft a, the outer diameter of the stator D_o, and the groove depth h_s were selected as the main optimization variables, and the groove width b_{s0} and groove bottom width b_{s2} were taken as 2.7mm and 5.8mm respectively on the basis of the experimental design results of the field.

4.3 Response Surface Method

The response surface method is mainly a method to find the mathematical law between the experimental target and each influencing factor, and to find the optimal value of each factor level.

ISSN: 2414-1895 DOI: 10.6919/ICJE.202506_11(6).0026

Firstly, the values of the optimization variables are divided into high level 1, central value 0, and low level -1. Table 5 shows the value range of the remaining optimization variables selected according to the Taguchi method.

Table 5. Optimize variable level values

Optimize variables	-1	0	1
a	16	16.75	17.5
D_o	80	81	82
h_s	10	11	12

According to the BOX-Behnken design, the orthogonal test matrix of the design is shown in Table 6.

Table 6. Orthogonal test table and test results

Number of trials	Optimize variables			F_{ave}/mN·m	P_{fe}/W
	a/mm	D_o/mm	h_s/mm		
1	16	80	11	670.4573	9.2152
2	16.75	82	10	686.5683	8.6317
3	17.5	81	10	706.1674	9.6556
4	16	81	10	670.5988	8.2892
5	16	81	12	670.3569	9.8114
6	17.5	81	12	705.8767	11.4024
7	16.75	80	10	686.534	9.0525
8	16.75	81	11	686.4216	9.5546
9	17.5	80	11	705.9976	10.7117
10	16.75	81	11	686.4216	9.5546
11	16.75	82	12	686.3151	10.1058
12	16.75	81	11	686.4216	9.5546
13	16.75	80	12	686.2285	10.7979
14	16	82	11	670.5021	8.7339
15	17.5	82	11	706.0526	10.1736

The equations of the optimization variable obtained by the response surface method and the response surface equation of the two optimization objectives.

$$\begin{aligned} F_{ave} =& 1191.2 - 85.663a + 0.448D_o - 0.785h_s \\ &+ 3.26158a^2 - 0.00384D_o^2 - 0.00629h_s^2 \\ &+ 0.0034a \cdot D_o - 0.01627a \cdot h_s + 0.01307D_o \cdot h_s \end{aligned} \quad (4)$$

ISSN: 2414-1895 DOI: 10.6919/ICJE.202506_11(6).0026

$$P_{fe}=55.1-7.14\cdot a-0.12D_o+3.143h_s+0.2637a^2 +0.00566D_o+0.08671h_s^{\,2}-0.0189a\cdot D_o +0.0749a\cdot h_s-0.06783D_o\cdot h_s \quad (5)$$

4.4 Optimization of Motor Parameters based on Egret Group Optimization Algorithm

The egret swarm optimization algorithm is a heuristic algorithm that combines the predatory behavior of snow egrets and great egrets. It is mainly composed of three aspects: the sitting and waiting strategy, the aggressive strategy and the discriminant condition. Before using the egret swarm optimization algorithm, it is necessary to set the variables.

First, the population size of the optimization algorithm is set to 100, and the maximum number of iterations is 200. Secondly, the fitting formulas (4) and (5) of the maximum output torque and stator iron consumption of the high-speed permanent magnet synchronous motor with the response surface method and the long axis length a, the outer diameter of the stator and the groove depth hs obtained by the response surface method are used as the optimization objective functions. Finally, the optimization variables and their constraints are shown in Table 4. The resulting Pareto front map and the selection points are shown in Figure 13.

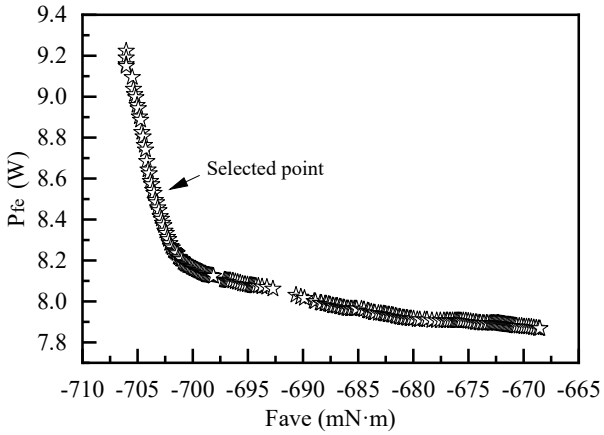

Figure 13. Pareto Frontier Diagram

As can be seen from Figure 13, with the decrease of stator iron consumption, the output torque of the new rotor structure permanent magnet synchronous motor also decreases, so the selection of optimization variables should be reasonable, and the influence of the size of the optimization variable on the output torque and stator iron consumption is coordinated with each other. The optimization data show that the egret group optimization algorithm can not only effectively reduce the stator iron consumption of the motor, but also increase the output torque of the motor, which can better achieve the purpose of multi-objective optimization.

The selected point on the Pareto front edge diagram is the optimal combination of parameters predicted by the algorithm is (17.5, 82, 10), the average output torque of the motor is 702.89mN·m, and the stator iron consumption is 8.54W. The finite element simulation model was established by using the predicted data, and the optimization results after the final solution were compared with the original data, and the comparison results are shown in Table 7. According to the data in Table 7, the output torque of the new rotor structure permanent magnet synchronous motor is increased by 3.77% and the stator iron consumption is reduced by 16.1% compared with the initial design after the optimization algorithm of the multi-objective egret swarm optimization algorithm, which indicates that the multi-objective optimization design of the new rotor structure permanent magnet synchronous motor is optimized by using the Egret swarm optimization algorithm.

ISSN: 2414-1895 DOI: 10.6919/ICJE.202506_11(6).0026

Table 7. Comparison of parameters before and after optimization

Parameter	Before	After
a	16.5	17.5
D_o	80	82
h_s	12	10
F_{ave}/mN·m	680.33	706.19
P_{fe}/W	10.56	8.86

5. Conclusion

In this paper, a new type of permanent magnet synchronous motor with rotor structure is studied, which uses the shape freedom of the bonded magnet to produce convex polarity by using an asymmetrical cross-section rotating shaft. Firstly, the torque characteristics of the motor are analyzed theoretically, then the motor is designed for simulation verification, and finally the motor is optimized, and the following conclusions are obtained:

(1) Through the theoretical analysis of the torque characteristics of the permanent magnet synchronous motor of the new rotor structure, it is determined that the new rotor structure can improve the output torque of the motor by using the reluctance torque.

(2) The electromagnetic finite element simulation software is used to model and simulate the motors of different structures, and the simulation results of the torque characteristics are consistent with the theoretical analysis, and the output torque of the new rotor structure motor is increased by 14.21% compared with the traditional basic structure motor.

(3) Using the egret group optimization algorithm to optimize the motor with multiple objectives, although the output torque is only 3.77% higher than the original design, the iron consumption of the stator is significantly reduced, reaching 16.1%, and the motor performance has been significantly improved.

References

[1] WANG Fengxiang, ZHANG Zhuoran. Design and control of permanent magnet synchronous motor[M]. Beijing: China Machine Press, 2018.

[2] LI Liyi, LIU Weiguo. Survey on Torque Ripple Suppression Technology for Permanent Magnet Synchronous Motor[J]. Proceedings of the CSEE, 2019, 39(6): 1785-1798.

[3] Zhu Z Q, Howe D. Electrical machines and drives for electric, hybrid, and fuel cell vehicles[J]. Proceedings of the IEEE, 2007, 95(4): 746-765.

[4] ZHANG Chenghui, LI Ke. Torque ripple analysis and suppression method of permanent magnet synchronous motor[J]. Transactions of China Electrotechnical Society, 2020, 35(10): 2123-2135.

[5] ZHAO Zhengming, CHEN Junling. Design and Optimization of Rotor Structure of Novel Permanent Magnet Synchronous Motor[J]. Proceedings of the CSEE, 2021, 41(3): 987-996.

[6] LIU Guohai,CHEN Zhihui. Torque Performance Optimization of Permanent Magnet Synchronous Motor Based on Finite Element Analysis[J]. Journal of Electrical Engineering & Control, 2022, 26(2): 45-53.

[7] DING Jialu, YU Shenbo, ZHAO Haining, et al. Optimization method for magnetic pole shape of surface-mount permanent magnet synchronous motor[J]. Micro & Special Electrical Machinery, 2020, 48 (09): 18-21+25.

[8] Performance optimization of surface-mounted permanent magnet pole synchronous motor for convex pole shoes[J]. Mechanical Science and Technology, 2019, 38 (10): 1514-1518.

[9] J. Chen et al., "Torque Enhancement of Surface-mounted Permanent Magnet Synchronous Machines via Axial Assisted Magnets," 2022 Second International Conference on Sustainable Mobility Applications, Renewables and Technology (SMART), Cassino, Italy, 2022, pp.

ISSN: 2414-1895 DOI: 10.6919/ICJE.202506_11(6).0026

[10] T. Kosaka, C. Higashihama, T. Ishihara, H. Matsumori,N. Matsui. Design Study on Light-weight Quasi-coreless SPMSM using CFRP, Small Amount of SMC Core and Aluminum Winding[J]. ICPE(ISPE),2023.

[11] Koji Yamaguchi,Tomoya Yamamoto,Naoki Omura.Torque Enhancement of Surface Permanent Magnet Motors utilizing Reluctance Torque for High-speed Motors with Bonded Magnets. The 2022 International Power Electronics Conference. IPEC-Himeji 2022 -ECCE Asia.